




# Local coordination of epithelial planar polarity in the maintenance and regeneration of the adult rat airway

Seiji Oyagi<sup>1,5</sup> · Ryosuke Nakamura<sup>2</sup> · Tatsuya Katsuno<sup>3</sup> · Tohru Sogami<sup>4</sup> · Yoshitaka Kawai<sup>5</sup>  · Yo Kishimoto<sup>5</sup> · Koichi Omori<sup>5</sup>

Received: 20 March 2023 / Accepted: 5 July 2023

© The Author(s), under exclusive licence to Springer-Verlag GmbH Germany, part of Springer Nature 2023

## Abstract

The maintenance of planar polarity in airway multiciliated cells (MCCs) has been poorly characterized. We recently reported that the direction of ciliary beating in a surgically inverted tracheal segment remained inverted beyond the time required for the turnover of cells, without adjustment to global distal-to-proximal polarity. We hypothesized that the local maintenance of tissue-level polarity occurs via locally reproduced cells. To provide further insight regarding this hypothetical property, we performed allotransplantation of an inverted tracheal segment between wild-type (donor) and tdTomato-expressing (host) rats, with and without scratching the mucosa of the transplants. The origin of cells in the transplants was assessed using tdTomato-specific immunostaining. Ciliary movement and structures were observed by high-speed video and electron microscopy to analyze MCC orientations. Variabilities in the orientations of closely and distantly located MCCs were analyzed to evaluate the local- and broad-scale coordination of polarity, respectively. The epithelium was maintained by donor-derived cells in the non-scratched inverted transplant over 6 months, beyond one cycle of turnover. The inverted orientation of MCCs was also maintained throughout the non-scratched transplant. MCCs regenerated in the scratched transplant were derived from the host and exhibited diverse orientations across the transplant. However, the orientations of adjacent regenerated MCCs were often coordinated, indicating that airway MCCs can locally coordinate their orientations. A steady-state airway may maintain MCC orientation by locally reproducing MCCs via the local coordination of polarity. This local coordination enables the formation and maintenance of tissue-level polarity in small regions after mucosal injury.

**Keywords** PCP · Cilium · Trachea · Airway · Regeneration

## Introduction

Mucus transportation is essential for the maintenance of airway homeostasis. The mucus stream is generated by the ciliary movement of multiciliated cells (MCCs), which predominantly cover the apical surface of the airway epithelium. In the trachea, cilia are oriented toward the oral side. Ciliary beating toward the oral side enables the excretion of inhaled pathogens from the lower respiratory tract along with the mucus (Randell et al. 2006). A disruption to the coordinated orientation of the cilia leads to coughing- and sneezing-like symptoms in mice (Kunimoto et al. 2012). Dysfunctional airway cilia, putatively including an uncoordinated ciliary stroke, are associated with various respiratory diseases such as chronic obstructive pulmonary disease, cystic fibrosis, and chronic rhinosinusitis (Tilley et al. 2015; Vladar and Königshoff 2020).

✉ Yoshitaka Kawai  
y\_kawai@ent.kuhp.kyoto-u.ac.jp

<sup>1</sup> Department of Otolaryngology-Head and Neck Surgery, Kyoto Min-iren Chuo Hospital, Kyoto, Japan

<sup>2</sup> Department of Rehabilitation Medicine, New York University Grossman School of Medicine, New York, USA

<sup>3</sup> Center of Anatomical, Pathological and Forensic Medical Researches, Graduate School of Medicine, Kyoto University, Kyoto, Japan

<sup>4</sup> Department of Otolaryngology-Head and Neck Surgery, SOSEIKAI hospital, Kyoto, Japan

<sup>5</sup> Department of Otolaryngology-Head and Neck Surgery, Graduate School of Medicine, Kyoto University, 54 Kawahara-cho, Shogoin, Sakyo-ku, Kyoto 606-8507, Japan

The direction of cilium is determined by the positional relationship between the basal body and basal foot, protein structures anchoring the cilium to the cytoskeleton (Boisvieux-Ulrich et al. 1985). In the trachea, the basal foot is typically attached to the oral side of the basal body, directing the ciliary stroke toward the oral side. The ability to coordinate the orientation of cellular structures along a tissue plane is called planar cell polarity (PCP). Epithelial PCP is observed in multiple organs, including the inner ear and hair follicles, as well as the oviduct and brain ventricles which have MCCs (Guo et al. 2004; Curtin et al. 2003; Landin Malt et al. 2019). PCP is regulated by the biased distribution of transmembrane proteins and their downstream signals (Srivastava et al. 2012; Vladar et al. 2012; Kunimoto et al. 2012).

The molecular mechanisms of PCP signaling have frequently been investigated in *Drosophila* (Lavalou and Lecuit 2022). Multiple pathways, such as core PCP, Fat/Ds, Fat2/Lar, and Toll-8/Cir1, have been identified as determinants of planar polarity in the developing bristles, hairs, and ommatidia of *Drosophila* (Lawrence et al. 1972; Nübler-Jung 1987; Cho et al. 2022; Barlan et al. 2017; Lavalou et al. 2021). The core PCP pathway, the most extensively investigated pathway, drives asymmetrical distribution of sets of “core proteins”; transmembrane proteins Vang and Frizzled (Fz) localize to opposite sides within a cell, to form protein complexes with Flamingo and Prickle in the Vang side and with Flamingo, Dishevelled, and Diego in the Fz side. This leads to dynamic changes in cytoskeleton alignment and the asymmetric distribution of cellular structures (Goodrich and Strutt 2011). Along with the formation of intracellular planar polarity, intercellular Vang–Fz interaction reinforces the polarity of adjacent cells, contributing to the expansion of planar polarity at the tissue level (Wallingford 2010; Lavalou and Lecuit 2022). Other PCP pathways likely similarly rely on asymmetrical intracellular protein distribution and intercellular communication, regulating planar polarity independently and/or by interacting with the core PCP pathway. Beyond the intercellular mechanism to locally determine tissue-level polarity, broader scale regulation is important for global planar polarity throughout the entire organ. The Fat/Ds pathway most likely drives global planar polarity in *Drosophila*. However, its interaction with other PCP pathways and relative contribution to global polarity is still controversial (Yang et al. 2002; Goodrich and Strutt 2011; Brittle et al. 2022). In addition, the initial cue to induce normal planar polarity remains elusive.

Although research regarding PCP signaling in mammals lags behind *Drosophila*, similar mechanistic roles of the core PCP pathway have been suggested (Deans 2021; Lavalou and Lecuit 2022). The biased distribution of Vangl (the mammalian ortholog of Vang) and Fz is also critical for the development of intracellular PCP in airway MCCs. In vitro ciliogenesis models have shown

that differentiating MCCs distribute the core PCP proteins asymmetrically in the early phase of differentiation, before the formation of immature cilia with poorly coordinated orientations (Vladar et al. 2016). As cilia mature in the later phase, further accumulation of the core PCP proteins intensifies the asymmetric protein distribution, leading to intracellular coordination of ciliary orientations. However, the intercellular mechanisms that regulate tissue-level polarity in the airway epithelium remain to be elucidated. Additionally, most of the current knowledge on the PCP of airway MCCs is based on in vitro and developmental studies. Further in vivo investigations using adult animal models are required to fully understand airway planar polarity.

The maintenance and regeneration of the airway epithelial planar polarity are essential for the retention of efficient mucociliary clearance throughout the lifespan. We previously performed auto-transplantation of inverted tracheal segments (Tsuji et al. 2018) and reported that the ciliary orientations in the transplant area remained inverted 6 months after transplantation, beyond the time for turnover of tracheal epithelial cells (Blenkinsopp 1967). No profound morphological changes were observed in the epithelium of the inverted segment after transplantation. These results imply that MCCs were locally maintained during turnover, and the orientations of the locally reproduced cells followed local tissue-level polarity rather than broad-scale lung-to-oral polarity. In contrast, our preliminary study with human subjects showed that tracheal MCCs which regenerated after irradiation damage were uncoordinated in their orientation (Nakamura et al. 2020). Based on these findings, we hypothesize that the steady-state airway epithelium maintains tissue-level polarity via intercellular mechanisms driving the local coordination of MCC polarity, similar to the intercellular PCP signaling in *Drosophila*.

In this study, we sought to provide further insights into the possible properties of the airway epithelium that facilitate the local maintenance of a steady-state epithelium and coordination of tissue-level polarity. Initially, we performed allotransplantation of an inverted tracheal segment from wild-type to tdTomato-expressing rats; we aimed to confirm that the epithelial cells in the transplant were maintained by the donor cells. Secondly, tracheae that were scratched, to remove the mucosa and disrupt the local reproduction of epithelial cells, were similarly transplanted. The orientations of regenerated host-derived MCCs in the scratched transplant were analyzed to assess polarity created by cells migrated from a distant part. The variability in the MCC orientation was compared between MCCs in close and distant regions to explore the local and broad-scale coordination of tissue-level polarity. This study potentially provides a foundation for future therapeutic approaches to maintain or improve the airway mucociliary function.

## Material and methods

### Animals

Wild-type (WT) Long-Evans rats were obtained from Japan SLC (Shizuoka, Japan). Transgenic Long-Evans rats ubiquitously expressing tdTomato (Flame rat: LE-Tg(Gt(ROSA)26Sor-CAG-tdTomato)9Jfhy) were provided by the National BioResource Project Rat (Kyoto, Japan) (Igarashi et al. 2016). Protocols for all animal experiments were approved by the Animal Research Committee of Kyoto University Graduate School of Medicine. Animal care was provided by the Institute of Laboratory Animals at Kyoto University.

### Allogenic transplantation of inverted tracheal segments

WT and heterozygous Flame rats were mated to generate littermates. Allogenic tracheal transplantation was performed between WT (donor) and flame (host) littermates of the same sex at age 8 weeks or older. All surgeries were performed under general anesthesia induced by an intraperitoneal injection of butorphanol tartrate (0.25 mg/100 g), medetomidine hydrochloride (0.015 mg/100 g), and midazolam (0.2 mg/100 g). The non-scratched and scratched inversion models were transplanted using the following method: the skin and subcutaneous tissues were incised in the host Flame rat and the submandibular glands and strap muscles were separated to expose the trachea; an approximately 2-mm incision was made in the anterior tracheal wall, and three tracheal cartilages were removed (Fig. 1a); the tracheal segment was removed from the donor WT rat using the same procedure; for the non-scratched inversion model, the extracted tracheal segment was inverted and transplanted into the tracheal defect in the flame rat immediately after its removal from the WT rat (Fig. 1a', b); for the scratched inversion model, the tracheal segment was scratched using KimWipes (NIPPON PAPER CRECIA CO, Tokyo, Japan) prior to inverted transplantation (Fig. 1c) to remove the donor epithelial cells and subepithelial tissues, including the subepithelial gland (Fig. 1d-f'''); tracheal cartilage and annular ligaments were left in the scratched trachea; the tracheal segment was sutured to the host trachea using 9-0 proline; the skin was closed using 5-0 nylon. Rats were euthanized using CO<sub>2</sub> exposure at post-operative days (POD) 1, 3, 7, and 14 and post-operative months (POM) 1 and 6. Tracheae were collected, as described below. For experiments related to analysis of MCC orientations, the orientations of tracheal samples were visually confirmed. Samples were trimmed into rectangular shapes with their lung–oral axis being the long side and their right–left axis

being the short side. In addition, the samples were incised at the lung-side right end to keep their orientations recognizable during experimental procedures.

### Analysis of ciliary beating directions

The ciliary beating directions were analyzed at POM6, as previously reported (Tsuji et al. 2018; Nakamura et al. 2020). In order to label the cilia, tracheae were treated with 8 µg/mL fluorescein isothiocyanate-conjugated wheat germ agglutinin (Vector Laboratories, Burlingame, CA, USA) for 1 h. Ciliary movement was observed under an upright microscope (model BX51, Olympus, Tokyo, Japan) and recorded at 50 frames/s using FASTCAM mini UX50 (Photron, Tokyo, Japan). A 50 × 50 µm square was defined as the region of interest (ROI). At least ten ROIs, 50 µm apart, were set throughout the non-transplant and transplant regions of individual rats. The beating directions of individual MCCs were measured using ImageJ software (National Institutes of Health, Bethesda, MD, USA) (Tsuji et al. 2018). Single and multiple ROI data were analyzed to interrogate the local and broad-scale regulation of polarity.

### Whole-mount immunofluorescence staining

#### Confirmation of epithelial cell removal and evaluation of cell origin in transplant

Tracheal samples were obtained at POM1 and POM6. Following fixation with 4% paraformaldehyde (PFA) in phosphate-buffered saline (PBS) for 30 min on ice and rinsing with PBS, the samples were treated with 1.0% Triton X-100 in PBS for 1 h at room temperature. Nonspecific antibody binding was blocked by incubation with 1.0% bovine serum albumin (BSA) in PBS for 1 h at room temperature. The samples were reacted with primary antibodies (rabbit anti-RFP, × 1000, ROCKLAND, PA, USA; mouse anti-acetylated α-tubulin, × 1000, Sigma Aldrich, MN, USA; rabbit anti-CK5, × 1000, Abcam, Cambridge, UK) at 4 °C and rinsed with PBS, followed by labeling with secondary antibodies (Alexa Fluor 555 and 647, Invitrogen, Waltham, MA) overnight at 4 °C. The samples were mounted using Fluoromount-G (Thermo Fisher Scientific, Waltham, MA, USA) and observed under a TCS SPE confocal microscope (Leica Microsystems, Wetzlar, Germany).

#### Localization of core PCP proteins

Following fixation with 10% trichloroacetic acid for 20 min on ice, tracheal samples harvested at POM1 were rinsed with 4-(2-hydroxyethyl)-1-piperazineethanesulfonic acid (HEPES)-buffered saline containing 0.05% Tween 20 and 5 mM calcium chloride. Mucosae were peeled from the

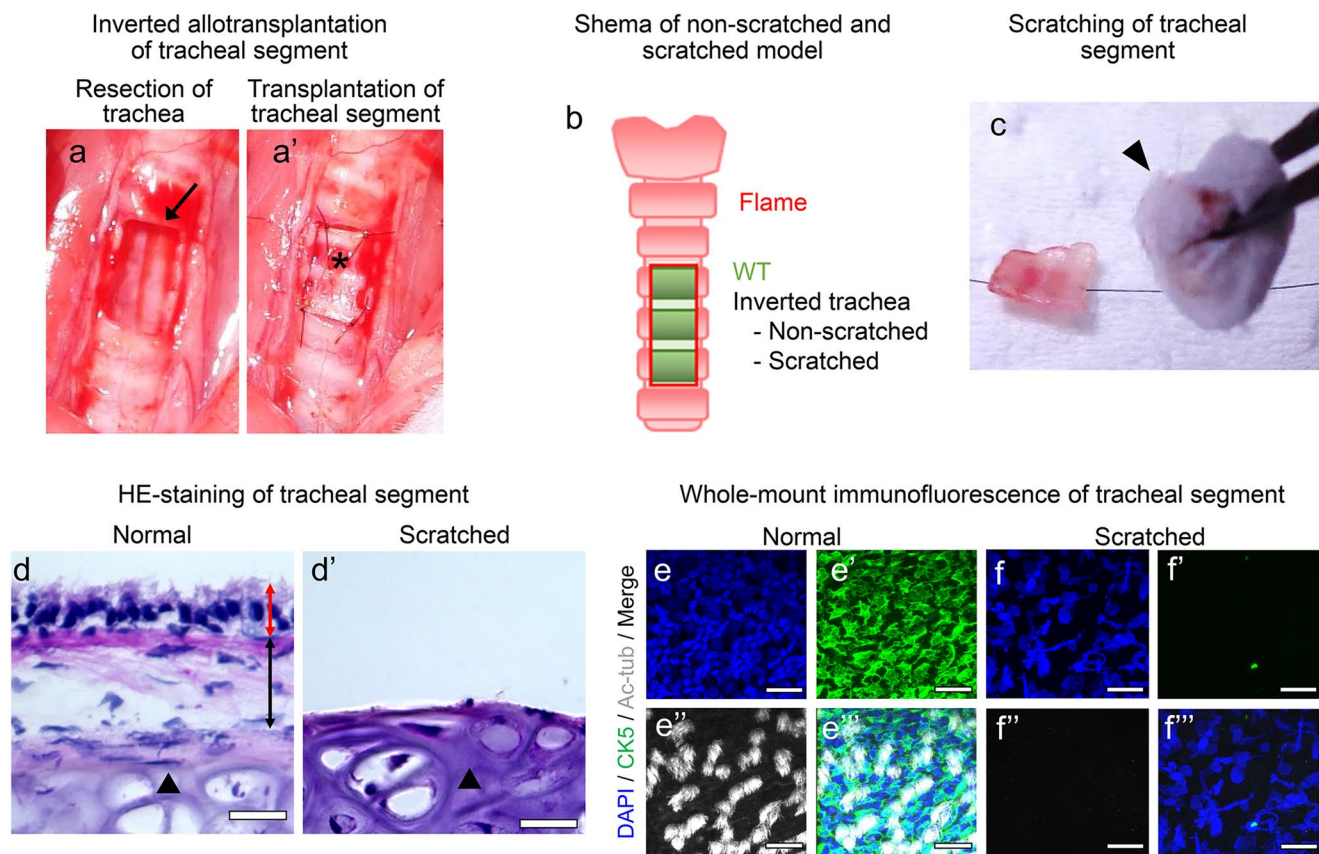


**Fig. 1** Inverted allotransplantation of non-scratched and scratched tracheae. **a–a'** Inverted allotransplantation of tracheal segment. The trachea of the flame rat was partially removed (**a**, arrow). The tracheal segment of the WT rat (\*) was transplanted into the flame rat in an inverted orientation (**a'**). **b** Schema of non-scratched and scratched model. This study employed non-scratched and scratched models, which were created by allotransplantation of non-scratched and scratched inverted tracheal segments. **c** Scratching of tracheal segment. In the scratched model, the luminal surface of the tracheal segment (arrow) was scratched using KimWipes (arrow head) before

transplantation. **d–d'** HE staining of tracheal segment. HE-stained cryosections of normal and scratched tracheal segments are shown. The epithelium (red double-headed arrow) and subepithelial tissue (black double-headed arrow) were observed in the normal tracheal (**d**) but removed by scratching (**d'**). The tracheal cartilage (arrowhead) was left in the scratched tracheal segment (**d'**). Scale bar = 30  $\mu$ m. **e–f''** Whole-mount immunofluorescence of normal and scratched tracheal segment. Cytokeratin 5 (CK5)-positive basal cells and acetylated  $\alpha$ -tubuline (Ac-tub)-positive MCCs were removed by scratching. Scale bar = 20  $\mu$ m

tracheal samples and blocked in 1% BSA in PBS containing 0.05% Tween 20 for 30 min. Subsequently, the samples were incubated with primary antibodies (rabbit anti-Vangl1,  $\times 200$ , Atlas Antibodies, Stockholm, Sweden; goat anti-Fz6,  $\times 50$ , R&D Systems, Minneapolis, MN, USA) overnight at 4  $^{\circ}$ C. After rinsing with HEPES-buffered saline, the samples were incubated with secondary antibodies (Alexa Fluor 488 and 647; Invitrogen) for 2 h at room temperature. Samples were inspected using an SP8 confocal microscope (Leica Microsystems).

### Immunofluorescence and HE staining of cryosection

Tracheal samples were embedded in an optimal cutting temperature compound. Sagittal cryosections were cut to

a thickness of 10  $\mu$ m and then fixed with 4% PFA in PBS for 10 min at room temperature and washed with PBS. Following treatment with 0.2% Triton X-100 for 5 min at room temperature to allow permeabilization, the samples were blocked with 1.0% BSA in PBS for 20 min at room temperature. They were incubated with primary antibodies (rabbit anti-RFP,  $\times 200$ , mouse anti-acetylated  $\alpha$ -tubulin; rabbit anti-CK5  $\times 200$ ) overnight at 4  $^{\circ}$ C, rinsed with PBS, and then labeled with secondary antibodies (Alexa Fluor 488, 555, and 647) overnight at 4  $^{\circ}$ C. The samples were mounted on Fluoromount-G mounting medium. TCS SPE was used for the observation of the samples.

For HE staining, PFA-fixed cryosections were stained with Mayer's hematoxylin solution for 3 min and eosin for 1 min, dehydrated with 70%, 80%, 90%, and 100% ethanol

and then immersed in xylene. The specimens were mounted on MOUNT-QUICK mounting medium (Daido Sangyo, Tokyo, Japan). Images were obtained using a BIOREVO BZ-9000 fluorescence microscope (KEYENCE).

### Scanning electron microscopy and array tomography

Ciliogenesis was assessed by scanning electron microscopy (SEM), as previously described (Tsuji et al. 2018). Samples were collected at PODs 1, 3, 7, and 14, and POMs 1 and 6. After fixation with 2.5% (w/v) glutaraldehyde, the tissues were dehydrated using ethanol, immersed in tert-butyl alcohol, and lyophilized. The samples were then sputter-coated with a platinum–palladium alloy using an IB-3 ion coater (Eiko, Tokyo, Japan) and inspected under an S-4700 scanning electron microscope (Hitachi, Tokyo, Japan).

Backscattered electron scanning electron microscopy (BSE-SEM) was performed to analyze the orientation of the basal foot at POM6. Samples were fixed with 2.5% (w/v) glutaraldehyde for at least 48 h. The fixed specimens were dehydrated with a series of dilutions of ethanol (65%, 75%, 85%, 95%, 99%, and 100%) and propylene oxide and embedded in epoxy resin (LUVEAK-812, Nacalai). The blocks were sectioned using an ultramicrotome (ARTOS 3D, Leica) equipped with a diamond knife (Hist JUMBO, 45 degrees, DiATOME) to cut 250-nm serial sections. Serial sections were collected on a cleaned silicon wafer strip held using a micromanipulator (MN-153, NARISHIGE) for BSE-SEM. The sections were stained at room temperature using 3% (w/v) aqueous uranyl acetate (20 min) and Reynolds lead citrate (3 min). The sections were imaged using SEM (JSM-7900F; JEOL, Tokyo, Japan) supported by Array Tomography Supporter software (System in Frontier, Tokyo, Japan), which enables automated imaging. Images were aligned and ordered using Stacker NEO software (System in Frontier, Tokyo, Japan). Basal foot directions were assessed by observation of the positional relationships between the basal bodies and feet using ImageJ software.

### Data analysis

The lung–oral axis of the tracheal sample was visually determined based on the longitudinal axis of the trachea. The right–left axis was vertical to the lung–oral axis on the epithelial plane of the tracheal sample. Since all tracheal samples were the abdominal part of the trachea, the right–left axis of tracheal samples and animal bodies were nearly identical. The right, oral, left, and lung sides were defined as 0°, 90°, 180°, and 270°. The directions of ciliary beating and basal feet were expressed as 0°–360°. Direction data were categorized as follows: oral side, >45°, ≤135°; lung side, >225°, ≤315°; left side, >135°, ≤225°; and right side, >315°, ≤45°. Ratios of the number of MCCs in each

direction group were calculated; the data of the distribution of the directions was presented using a rose diagram illustrated using Octave (GNU General Public License; <https://www.gnu.org/software/octave/>). The mean and standard deviation (SD) of the direction data were calculated as previously described (Nakamura et al. 2020). The Mann–Whitney *U* test was performed to compare the SD and mean directions of the basal foot. Differences were considered to be statistically significant at  $p \leq 0.05$ .

## Results

### Origins and ciliary beating directions of MCCs in non-scratched inversion model

In the epithelium of the non-scratched inverted model, no morphological changes were observed across the non-transplanted and transplanted areas from POD14 to POM6 (Fig. 2a–a'''). At POM6, tdTomato-positive host cells were not found in the epithelium of the transplant, including in the basal layer where cytokeratin 5-positive basal progenitor/stem cells exist (Fig. 2b–e'''). Although our experimental model was unable to clarify whether donor epithelial cells migrated within the transplant, our results indicated dynamic migration from the host tissue to the transplant did not occur. To assess the broad-scale tissue-level polarity across the transplant, we evaluated ciliary beating directions in multiple ROIs, which were placed at least 50 μm away from each other. Nearly 90% of MCCs beat their cilia toward the lung side in the inverted transplant at POM6 (Fig. 2f–g'; Movie 1); this is similar to previous findings from the inverted auto-transplantation model (Tsuji et al. 2018). The locally reproduced cells likely maintained an inverted ciliary orientation.

### Origins and ciliary beating directions of MCCs in the scratched inversion model

The scratched inversion model was employed to induce penetration of host epithelial cells into the tracheal transplant. The luminal surface of the transplant was almost entirely covered by the newly formed epithelium by POD7 (Fig. 3a–a'); however, MCCs were sparsely distributed and their cilia were immature at this time point. As regeneration proceeded, the transplant area was largely covered by MCCs with apparently mature cilia at POM1, and the morphology of the regenerated epithelium was maintained over six months (Fig. 3a–a'''). Immunofluorescence examination revealed that the regenerated epithelium was formed by tdTomato-positive host cells (Fig. 3b–c'''). MCCs regenerated in the transplant did not necessarily beat toward the lung side (Movie 2); the ciliary beating directions measured in multiple ROIs highly deviated from the lung-side direction (Fig. 3d–e'). However, there were

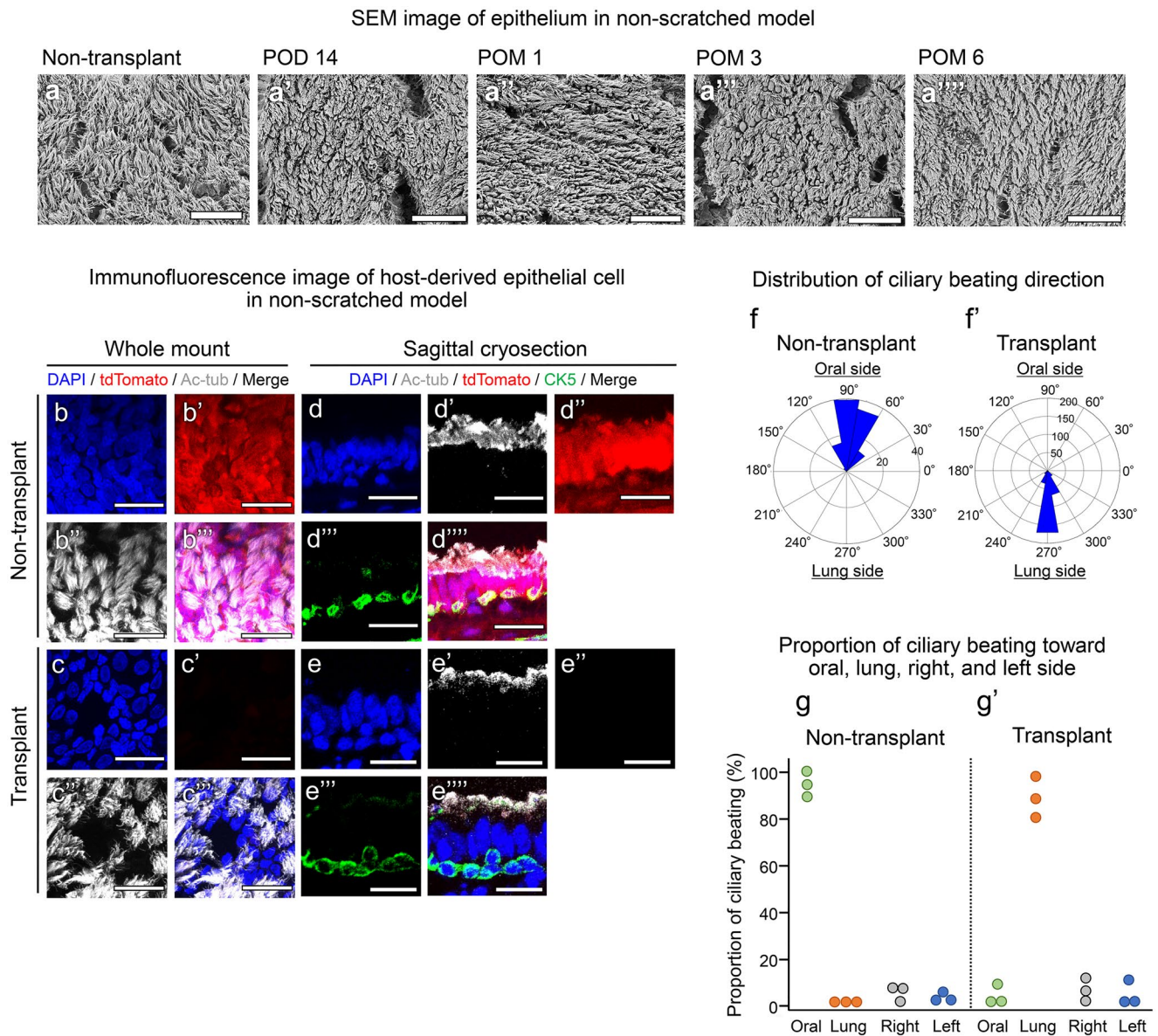


**Fig. 2** Morphology, cell origin, and ciliary beating direction in non-scratched inverted tracheal transplant. **a–a''''** SEM image of the epithelium in non-scratched model. Non-transplant and transplant areas at POD14, POM1, POM3, and POM6 are shown. Scale bar=30  $\mu$ m. **b–e''''** Immunofluorescence image of host-derived epithelial cell in non-scratched model. Cryosections and whole-mount tracheal samples were obtained at POM6. Flame rat-derived cells (host cells) and MCCs were stained using anti-tdTomato (red) and anti-acetylated tubulin (Ac-Tub; white) antibodies, respectively. The cryosections were also stained using anti-cytokeratin 5 (CK5, green) to observe

basal cells. Scale bar=20  $\mu$ m. **f–f''** Representative distribution of ciliary beating direction at POM6. Data were obtained from multiple 50 $\times$ 50  $\mu$ m ROIs. Non-transplanted area: 106 cells, 10 ROIs. Transplant area: 310 cells and 31 ROIs. **g–g'** Proportion (%) of ciliary beating directions toward the oral (>45°,  $\leq$ 135°), lung (>225°,  $\leq$ 315°), right (>315°,  $\leq$ 45°), and left (>135°,  $\leq$ 225°) side in total MCC observed across multiple ROI at POM6,  $N=3$ . Abbreviations: SEM, scanning electron microscopy; POM6, post-operative month 6; ROI, region of interest

no significant differences between the oral (40.2%  $\pm$  13.1%), lung (21.2%  $\pm$  18.0%), right (19.7%  $\pm$  4.1%), and left (19.0%  $\pm$  9.5%) directions ( $n=4$ ) (Fig. 3d–e'). These results indicate that the original planar polarity was lost in the regenerated epithelium; however, as shown in Movie 2, the MCCs in a single ROI seemed to beat their cilia in a similar direction.

### Local coordination of ciliary beating directions across regenerated MCCs

Next, we focused on assessing the local coordination of MCC orientation. The ciliary beating directions in each ROI were analyzed. In the non-scratched inversion model, ciliary

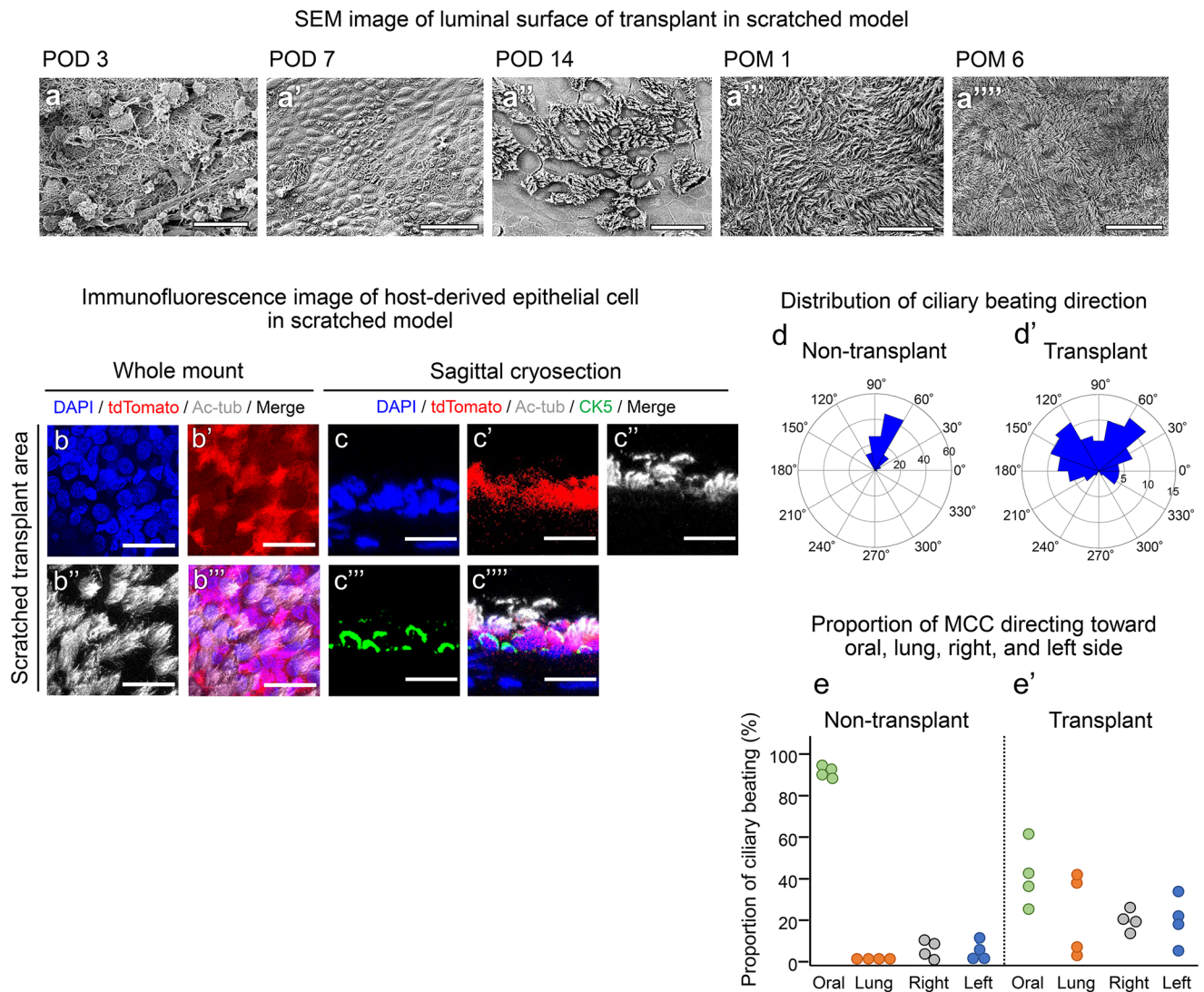


**Fig. 3** Morphology, cell origin, and ciliary beating direction in scratched inverted tracheal transplant. **a–a''''** SEM image of luminal surface of transplant in scratched model. Regenerative process of MCCs in scratched transplant at POD3, POD7, POD14, POM1, and POM6 is shown. Scale bar=30  $\mu$ m. **b–c''''** Immunofluorescence image of host-derived epithelial cell in scratched model. Cryosections and whole-mount tracheal samples were obtained at POM6. Flame rat-derived cells (host cells) and MCCs were stained using anti-tdTomato (red) and anti-acetylated tubulin (Ac-Tub; white) antibodies, respectively. The cryosections were also stained using anti-cytoker-

atin 5 (CK5, green) to observe basal cells. Scale bar=20  $\mu$ m. **d–d'** Representative distributions of ciliary beating direction at POM6. Data were obtained from multiple 50 $\times$ 50  $\mu$ m ROIs. The scales of the rose diagrams indicate the number of cells. Non-transplanted area: 107 cells, 10 ROIs. Transplant area: 94 cells and 18 ROIs. **e–e'** Proportion (%) of ciliary beating direction toward the oral (>45 $^{\circ}$ ,  $\leq$ 135 $^{\circ}$ ), lung (>225 $^{\circ}$ ,  $\leq$ 315 $^{\circ}$ ), right(>315 $^{\circ}$ ,  $\leq$ 45 $^{\circ}$ ), and left (>135 $^{\circ}$ ,  $\leq$ 225 $^{\circ}$ ) side in total MCC observed across multiple ROI at POM6,  $N=4$ . Abbreviations: SEM, scanning electron microscopy; POM6, post-operative month 6; ROI, region of interest

movement was predominantly directed toward the lung side in every ROI analyzed (Fig. 4a–a'''). In the scratched transplant, the distribution of the ciliary beating directions at each ROI was concentrated in a particular direction (Fig. 4b–b'''). The beating directions at each ROI were less diversified than those at multiple ROIs. The SDs of ciliary beating directions from the single- and multiple ROI datasets were evaluated to confirm the reduced diversity in the beating directions of

cilia from single ROIs. The SD calculated from the single ROI data in the scratched transplant was lower than that calculated from the multiple ROI data (Fig. 4c–c'). In addition, in the non-scratched model, the SD from the single ROI data was lower than that from multiple ROI data of the transplant and non-transplant areas. MCCs in close proximity were relatively highly coordinated in their orientations, both in regenerated and steady-state epithelia.

Distribution of ciliary beating direction in multiple- and single-ROI data

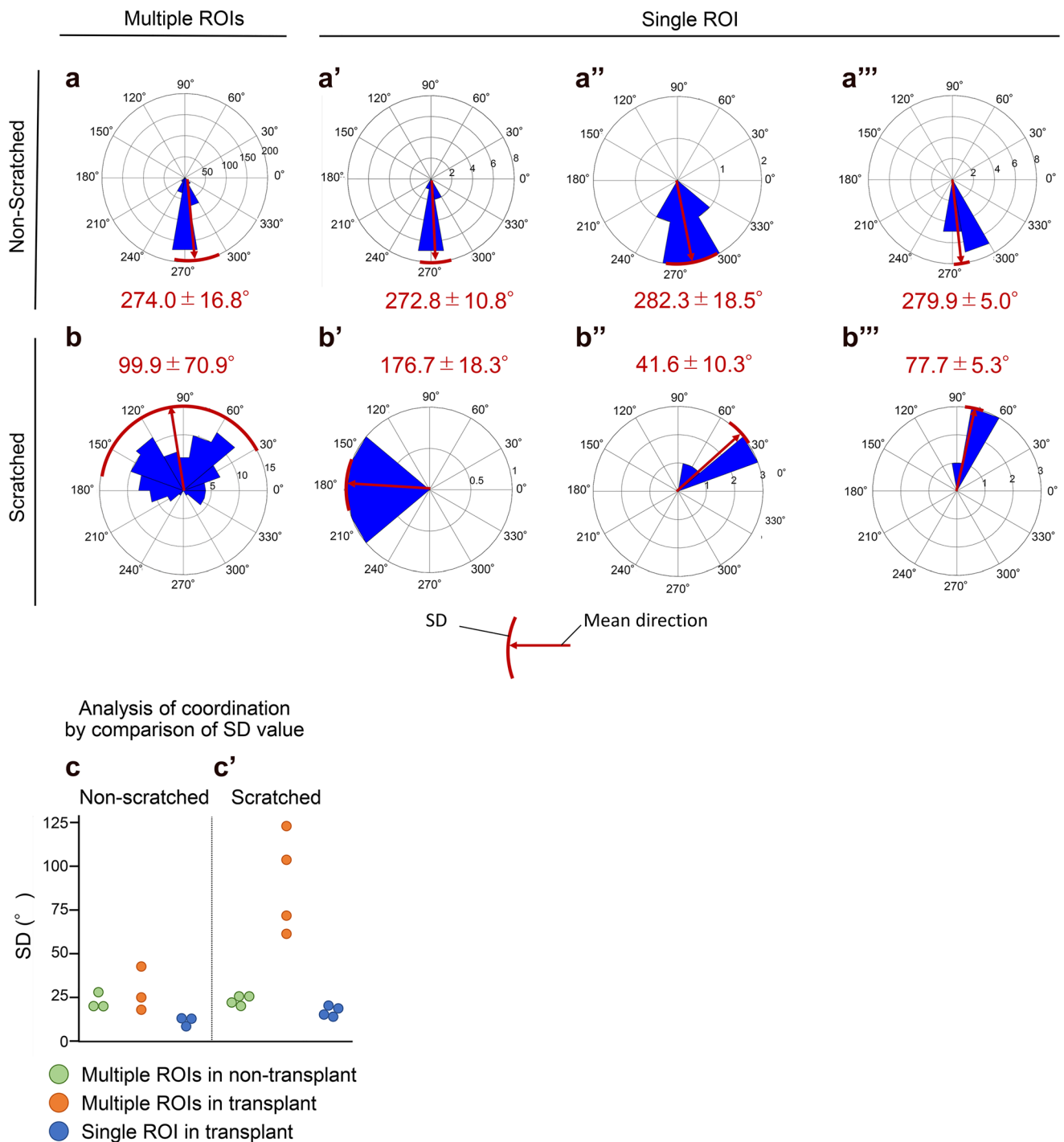


**Fig. 4** Coordinated ciliary beating directions across MCCs located in close proximity. **a–b'''** Distribution of ciliary beating direction in multiple and single ROI data. Representative distribution of ciliary beating directions at POM6 is shown. Rose diagrams illustrate multiple ROI data from each rat of non-scratched and scratched groups and single ROI data from three ROIs in each rat of non-scratched and scratched groups. The mean direction and SD are indicated by red arrows and red arcs, respectively. **c–c'** Analysis of coordination in ciliary beating direction by comparison of SD value. The data of

ciliary beating directions were collected from the multiple and single ROIs in the non-scratched and scratched models at POM6. SD values obtained from individual rats are plotted in the dot pots; the SD value of the multiple ROI data was calculated from all direction data obtained at multiple ROIs in each rat; the SD value of the single ROI data was the average of SDs independently calculated at individual ROIs in each rat.  $N=3$  (non-scratched),  $N=4$  (scratched). Abbreviations: POM6, post-operative month 6; ROI, region of interest; SD, standard deviation



## Localization of core PCP proteins

Since the core PCP pathway determines intracellular planar polarity and is putatively involved in the intercellular adjustment of polarity in MCCs (Lavalou and Lecuit 2022), Vangl1 and Fz6 were visualized using immunofluorescence after transplanting the scratched segment. Concentration of Vangl1- and Fz6-positive staining was observed in the transplant area (Fig. 5a–f). The alignment of Vangl1 and Fz6 appeared to be coordinated within each microscopic field, consistent with the results of the local coordination of the ciliary beating directions.

## Directions of basal feet

The basal structures of the cilia were observed using SEM and an array tomography technique to further detail the intracellular planar polarity and intercellular coordination of MCCs (Fig. 6a). Serial images obtained by array tomography displayed basal feet and bodies at the apical sections of the MCCs, and the arrangement of cells was more clearly observed at the middle sections (Fig. 6b, c). In the apical sections of the scratched transplant, basal feet within each MCC appeared to be well-coordinated in a certain direction, which confirms the polarization of the individual regenerated MCCs (Fig. 6d). Statistically, scratching damage to

the basal feet directions in individual MCCs was not fully recovered at POM6; the SD was higher in the transplant area than in the non-transplant area. However, the disparity was low, at approximately  $3^\circ$  (Fig. 6e). Because orientation cues from adjacent cells are the most likely determinants of tissue-level polarity (Lavalou and Lecuit 2022), we explored the better coordination of MCC orientations in adjacent MCCs than in MCCs that were 2 cells apart. MCC orientations were determined as mean basal foot directions in individual MCCs, and disparities in MCC orientations between adjacent MCCs, as well as between 2 cells apart MCCs, were measured. The mean disparity in MCC orientations was approximately of  $30^\circ$  between adjacent cells. This was significantly lower than the mean disparity in MCC orientations between MCCs that were 2 cells apart (Fig. 6f, g). This result confirms the efficient coordination of planar polarity between adjacent MCCs.

## Discussion

The conservation of the planar polarity of the airway epithelium is important for maintaining efficient mucus transportation. Despite recent advancements in the understanding of PCP, the regulatory mechanisms driving the maintenance of mammalian airway planar polarity have been poorly

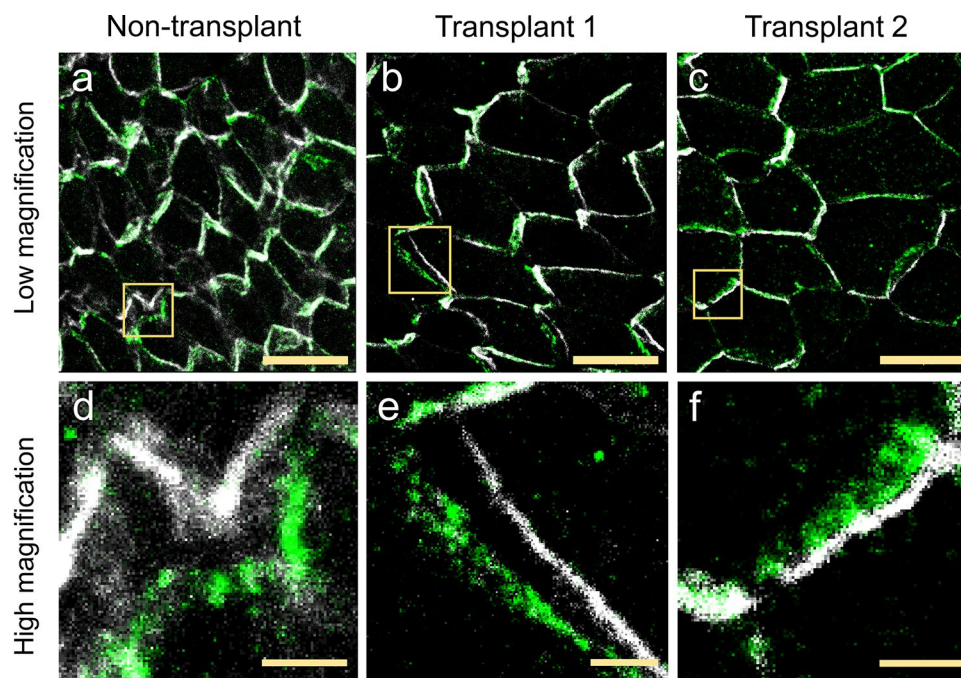


**Fig. 5** Localization of core PCP proteins in scratched transplant. **a–f** Whole-mount immunofluorescence images of Vangl1 (white) and Fz6 (green) in regenerated epithelium of scratched transplants at POM1. A region in the non-transplant (**a**) and two regions in the scratched transplant (transplant 1 and 2) are shown (**b**, **c**). Regions denoted as

rectangles in the low magnification images are magnified and shown as high magnification images below the low magnification images. Scale bar =  $10\ \mu\text{m}$  (**a**, **b**, **c**), Scale bar =  $2\ \mu\text{m}$  (**d**, **e**, **f**). Abbreviations: POM1, post-operative month 1

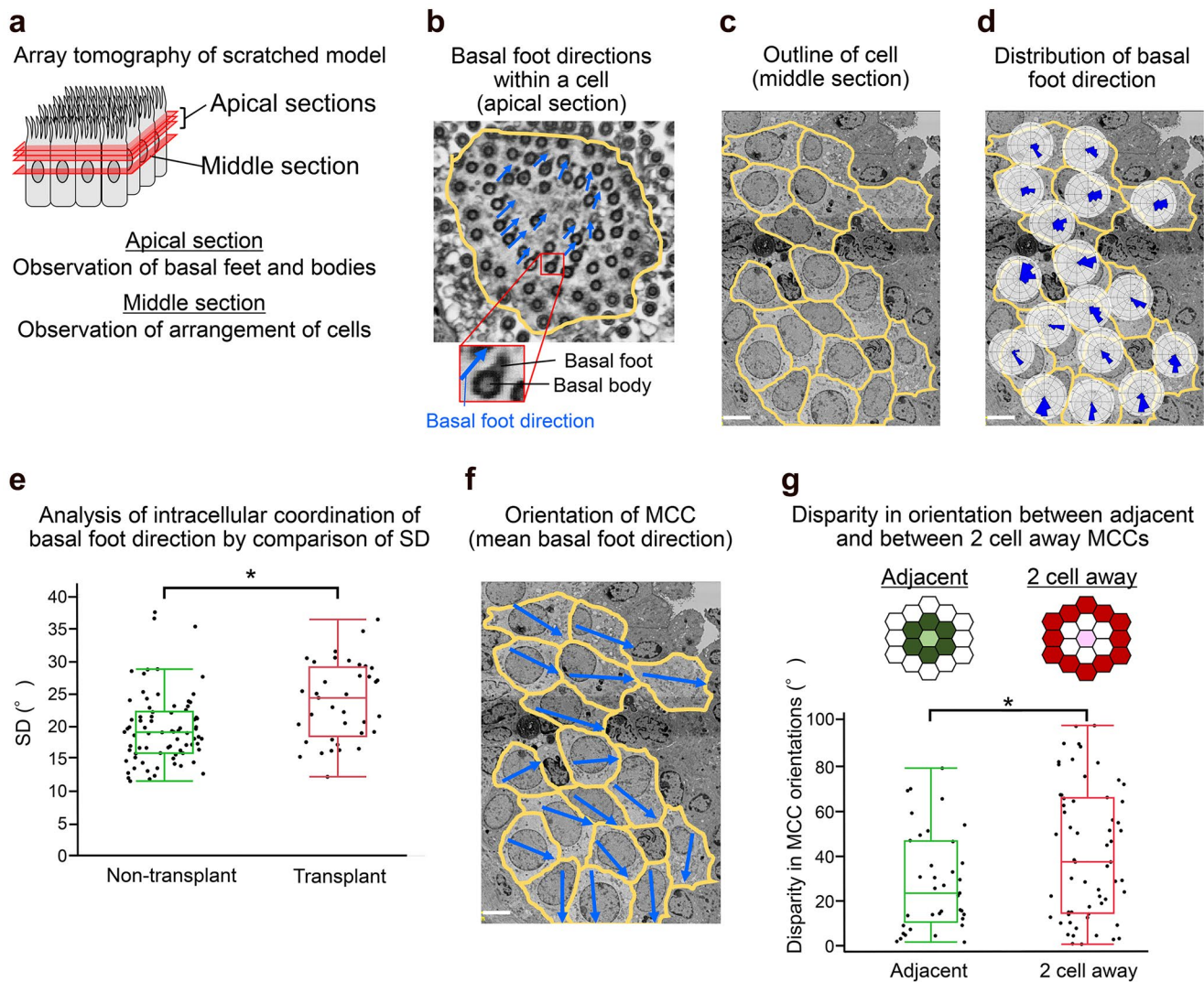


**Fig. 6** Basal foot directions in scratched transplant. **a** Schematic of array tomography of scratched model for observation of basal structure of cilium and location of MCC. Serial sections along the epithelial plane were obtained. Basal feet and bodies were observed at apical sections of the epithelium. Since the heights of epithelial cells were uneven, basal feet and bodies were inspected at multiple serial sections. Locations of cells were observed at a middle section. **b–d** SEM image obtained by array tomography (POM6). **b** Basal foot directions within a cell. Basal feet and bodies are observed as triangular and round structures in the apical part of MCCs. Blue arrows indicate the direction of the basal feet. **c** Outline of cell. In the middle section, outlines of individual MCCs and nuclei are observed, and the locations of cells are more clearly observed than in the apical sections. The yellow lines illustrate the outlines of MCCs. Scale bar = 5  $\mu$ m. **d** Distribution of basal foot direction in each cell. Data of basal foot directions in individual MCCs were collected by inspecting serial sections. Rose diagrams illustrating the distributions of

basal foot directions are overlaid on corresponding MCCs in the SEM image. Scale bar = 5  $\mu$ m. **e** Analysis of intracellular coordination of basal foot direction by comparison of SD. Basal foot directions were measured at POM6, and SDs of basal foot directions in individual MCCs are plotted in the dot plots. Non-transplant area: 78 cells. Transplant area: 37 cells. \*Statistically significant difference between the groups (Mann–Whitney  $U$  test,  $p < 0.005$ ). **f** Orientations of MCCs. MCC orientations were determined as mean basal foot directions in individual MCCs and are denoted by blue arrows in the SEM image. Scale bar = 5  $\mu$ m. **g** Disparity in orientation between adjacent MCCs and between 2 cell away MCCs. The disparities in MCC orientations (mean basal foot directions) between adjacent and 2-cell away MCCs were measured for 37 and 61 pairs of cells, respectively, and plotted in the dot plots. \*Statistically significant differences between the groups (Mann–Whitney  $U$  test,  $p < 0.05$ ). Abbreviations: SEM, scanning electron microscopy; MCC, multiciliated cells; SD, standard deviation; POM6, post-operative month 6

discussed. The present study used tracheal allotransplantation models to examine the orientations of MCCs maintained or regenerated in the transplants, with an emphasis on local coordination, a putative mechanism for the maintenance of

tissue-level polarity. Although the current study did not clarify the specific mechanisms controlling tissue-level polarity, our findings confirmed that the tracheal epithelium locally coordinates the orientations of MCCs.

In the inverted transplant of the non-scratched model, the donor epithelial cells maintained their epithelium for a period longer than one cycle of turnover, which is reportedly 70–110 days (Blenkinsopp 1967), without the dynamic migration of epithelial cells (Fig. 2b–b''', d–d'''). In addition, the maintained donor MCCs beat toward the lung side in the non-scratched transplant (Fig. 2f–g'). This suggests that airway epithelial cells, including basal cells, were locally maintained without significant cell migration, and MCCs newly generated during epithelial cell turnover maintained the original polarity of the inverted transplant. In contrast, scratched transplants induced penetration of epithelial cells from the host tissue (Fig. 3b–c'''). The orientation of the regenerated MCCs was not coordinated in a particular direction across the transplant area (Fig. 3d–e'). This indicates that the MCCs regenerated at a distance from the host epithelium cannot adopt the planar polarity associated with the non-transplanted area. This finding is consistent with our previous report which showed that MCCs regenerated in an artificial tracheal graft failed to coordinate their orientations along the normal distal-to-proximal polarity seen outside the graft (Nakamura et al. 2021).

Despite the loss of broad-scale tissue-level polarity across the scratched transplant, the orientations of the regenerated MCCs in close proximity were coordinated, particularly between adjacent cells (Figs. 4 and 6f, g). This indicates that the adult airway epithelium has intercellular mechanisms that coordinate local tissue-level polarity. As shown in the SEM images, the differentiation of MCCs in the scratched transplant was initiated in separated areas, and the density of MCCs later increased (Fig. 3a–a'''). The initial cue directing the orientations of the isolated MCCs remains unclear; however, it is possible that the differentiated MCCs provide an orientation cue to the surrounding differentiating cells during epithelial regeneration to locally coordinate polarity. A plausible mechanism behind this local coordination might be the intercellular signals of the PCP signaling pathways. Although there are few studies on the intercellular mechanism of the core PCP signaling pathway in vertebrates, a previous report on the chick inner ear showed that the orientations of vestibular hair cells were guided by Vangl1 expressed by adjacent supporting cells. This therefore suggests that the intercellular mechanism of the core PCP signaling pathway exists in vertebrates (Warchol and Montcouquiol 2010).

However, tissue-level planar polarity is not simply regulated by PCP signaling pathways (Goodrich and Strutt 2011; Thomas and Strutt 2012; Barlan et al. 2017; Lavalou et al. 2021). Fluid shear stress is known to affect PCP in MCCs (Chien et al. 2015). An *in vitro* airway ciliogenesis model using pluripotent stem cells revealed that artificial fluid flow coordinates the orientation of airway MCCs with the flow direction (Sone et al. 2021). Based on the results of this

previous finding, the liquid flow generated by differentiated MCCs might indicate another possible orientation cue to adjust the polarity of differentiating neighbors. Further investigation is warranted to determine whether individual MCCs generate sufficient flow to alter the orientations of adjacent cells. Furthermore, additional research into the involvement of the PCP signaling pathways in coordinating the tissue-level polarity of the airway epithelium is required.

The epithelium in the non-scratched transplant, as in the normal airway, maintained a normal epithelial morphology and original tissue-level polarity. Since polarized mature MCCs exist around newly generated MCCs during turnover, maintenance of the original planar polarity would be feasible via this proposed local coordination mechanism in such intact airway epithelia. It would also be feasible that a similar polarity to the original is formed in regenerated MCCs after a small-scale epithelial injury, using support from uninjured neighboring MCCs. However, once tissue-level polarity is improperly formed after epithelial damage, an unfavorable polarity could similarly be maintained by the local coordination mechanism and persist, presumably over multiple cycles of epithelial turnover. Regarding the maintenance of PCP during epithelial turnover, murine basal keratinocytes transmit their core PCP proteins to daughter cells through trans-endocytosis during asymmetric cell division, a possible mechanism of epidermal PCP maintenance (Heck and Devenport 2017). However, in contrast to keratinocytes that have planar polarity before terminal differentiation, the asymmetric distribution of core PCP proteins is undetectable in airway basal stem/progenitor cells (Vladar et al. 2016). Therefore, orientation cues are more likely to be provided by MCCs than by basal cells in the airway.

Among the multiple mechanisms regulating PCP, morphogenetic forces have recently emerged as key to global cell alignment across organs (Lavalou and Lecuit 2022). Strains driven by collective cell movement and rearrangement of the cytoskeleton stimulate PCP signaling pathways in developing organs. Additionally, the parallel alignment of fibrils in the basement membrane has been suggested to serve as a fixed template for cell alignment by providing a platform for integrin and the dystrophin–dystroglycan complex (Cerqueira Campos et al. 2020). In the present study, the donor-derived mesenchymal tissues, such as tracheal cartilage and the intercondylar membrane, did not adjust the alignment of MCCs along the proximal–distal axis in the scratched model (Figs. 1d and 3c, d); this suggests that these tissues are unlikely to provide cues for epithelial planar polarity. Investigations of the airway basement membrane and lamina propria are necessary to understand the relationship between morphogenetic cues and MCC orientation.

Our study also provides insights into the formation of intracellular polarity within individual MCCs. The basal feet in each regenerated MCC were nearly unidirectional

(Fig. 6e), and the localization of Vangl1 and Fz6 in the regenerated epithelium was biased (Fig. 5a–f). Intracellular PCP mechanisms, including the core PCP pathway, were likely responsible for the successful organization of individual MCCs during epithelial regeneration, to almost normal cilium alignment. However, the SD of the mean basal foot directions of the individual regenerated MCCs was slightly higher than that of normal MCCs, even after 6 months of the recovery period (Fig. 6e). Given that the maturation of MCCs is closely related to the formation of intracellular planar polarity (Vladar et al. 2016), regeneration of completely mature MCCs may be difficult in such denuded tracheae.

In summary, our results confirm the local coordination of tissue-level planar polarity in the airway epithelium of adult rats after inverted tracheal transplant. Airway epithelial planar polarity was likely maintained by the local reproduction of MCCs during turnover in the steady-state epithelium. Although the regenerated epithelium after mucosal damage lost its original lung-to-oral polarity in the scratched tracheal transplant, MCCs in close proximity coordinated their orientations. Intercellular communication between adjacent cells is likely involved in the local coordination of tissue-level planar polarity. The maintenance of distal-to-proximal polarity in healthy airways would be feasible by the local coordination mechanism. In injured airway epithelia, this mechanism of local coordination may contribute to the formation and maintenance of tissue-level polarity in small regions; however, prolonged unfavorable planar polarity is formed after broad-scale damage.

**Acknowledgements** We thank Keiko Okamoto-Furuta and Haruyasu Kohda from the Division of Electron Microscopic Study, Center for Anatomical Studies, Graduate School of Medicine, Kyoto University, for their technical support in electron microscopy.

**Author contribution** SO, RN, YK, YK, and KO designed the study; SO, RN, and TK performed the experiments; SO and RN analyzed the data; SO and RN wrote the manuscript; and TS, YK, YK, and KO supervised the project. All authors have read and approved the final manuscript.

**Funding** This study was supported by the Japan Society for the Promotion of Science (JSPS) KAKENHI (20K18251) and GSK Japan Research Grant 2020 (A-33).

**Data availability** As a data availability statement, authors declare the data underlying this article are available in the article and in its online supplementary material.

## Declarations

**Ethics approval** All experimental protocols were approved by the Animal Research Committee of Kyoto University Graduate School of Medicine.

**Consent to participate** Not applicable.

**Competing interests** The authors declare no competing interests.

## References

- Barlan K, Cetera M, Horne-Badovinac S (2017) Fat2 and lar define a basally localized planar signaling system controlling collective cell migration. *Dev Cell* 40:467–477.e5. <https://doi.org/10.1016/j.devcel.2017.02.003>
- Blenkinsopp WK (1967) Proliferation of respiratory tract epithelium in the rat. *Exp Cell Res* 46:144–154. [https://doi.org/10.1016/0014-4827\(67\)90416-8](https://doi.org/10.1016/0014-4827(67)90416-8)
- Boisvieux-Ulrich E, Laine MC, Sandoz D (1985) The orientation of ciliary basal bodies in quail oviduct is related to the ciliary beating cycle commencement. *Biol Cell* 55:147–150. <https://doi.org/10.1111/j.1768-322X.1985.tb00417.x>
- Brittle A, Warrington S, Strutt H, Manning E, Tan S, Strutt D (2022) Distinct mechanisms of planar polarization by the core and Fat-Dachsous planar polarity pathways in the *Drosophila* wing. *Cell Rep* 40(13):111419. <https://doi.org/10.1016/j.celrep.2022.111419>
- Cerqueira Campos F, Dennis C, Alégot H, Fritsch C, Isabella A, Pouchin P, Bardot O, Horne-Badovinac S, Mirouse V (2020) Oriented basement membrane fibrils provide a memory for F-actin planar polarization via the dystrophin-dystroglycan complex during tissue elongation. *Development* 147. <https://doi.org/10.1242/dev.186957>
- Chien YH, Keller R, Kintner C, Shook DR (2015) Mechanical strain determines the axis of planar polarity in ciliated epithelia. *Curr Biol* 25:2774–2784. <https://doi.org/10.1016/j.cub.2015.09.015>
- Cho B, Song S, Wan JY, Axelrod JD (2022) Prickle isoform participation in distinct polarization events in the *Drosophila* eye. *PLoS One* 17:e0262328. <https://doi.org/10.1371/journal.pone.0262328>
- Curtin JA, Quint E, Tshipouri V, Arkell RM, Cattanch B, Copp AJ, Henderson DJ, Spurr N, Stanier P, Fisher EM, Nolan PM, Steel KP, Brown SD, Gray IC, Murdoch JN (2003) Mutation of *Celsr1* disrupts planar polarity of inner ear hair cells and causes severe neural tube defects in the mouse. *Curr Biol* 13:1129–1133. [https://doi.org/10.1016/S0960-9822\(03\)00374-9](https://doi.org/10.1016/S0960-9822(03)00374-9)
- Deans MR (2021) Conserved and divergent principles of planar polarity revealed by hair cell development and function. *Front Neurosci* 15:742391. <https://doi.org/10.3389/fnins.2021.742391>
- Goodrich LV, Strutt D (2011) Principles of planar polarity in animal development. *Development* 138:1877–1892. <https://doi.org/10.1242/dev.054080>
- Guo N, Hawkins C, Nathans J (2004) Frizzled6 controls hair patterning in mice. *Proc Natl Acad Sci USA* 101:9277–9281. <https://doi.org/10.1073/pnas.0402802101>
- Heck BW, Devenport D (2017) Trans-endocytosis of planar cell polarity complexes during cell division. *Curr Biol* 27:3725–3733.e4. <https://doi.org/10.1016/j.cub.2017.10.053>
- Igarashi H, Koizumi K, Kaneko R, Ikeda K, Egawa R, Yanagawa Y, Muramatsu S, Onimaru H, Ishizuka T, Yawo H (2016) A novel reporter rat strain that conditionally expresses the bright red fluorescent protein tdTomato. *PLoS One* 11:e0155687. <https://doi.org/10.1371/journal.pone.0155687>
- Kunimoto K, Yamazaki Y, Nishida T, Shinohara K, Ishikawa H, Hasegawa T, Okanou T, Hamada H, Noda T, Tamura A, Tsukita S, Tsukita S (2012) Coordinated ciliary beating requires Odf2-mediated polarization of basal bodies via basal feet. *Cell* 148:189–200. <https://doi.org/10.1016/j.cell.2011.10.052>
- Landin Malt AL, Dailey Z, Holbrook-Rasmussen J, Zheng Y, Hogan A, Du Q, Lu X (2019) Par3 is essential for the establishment of planar cell polarity of inner ear hair cells. *Proc Natl Acad Sci USA* 116:4999–5008. <https://doi.org/10.1073/pnas.1816333116>
- Lavalou J, Lecuit T (2022) In search of conserved principles of planar cell polarization. *Curr Opin Genet Dev* 72:69–81. <https://doi.org/10.1016/j.gde.2021.11.001>

- Lavalou J, Mao Q, Harmansa S, Kerridge S, Lellouch AC, Philippe JM, Audebert S, Camoin L, Lecuit T (2021) Formation of polarized contractile interfaces by self-organized Toll-8/Cir1 GPCR asymmetry. *Dev Cell* 56:1574–1588.e7. <https://doi.org/10.1016/j.devcel.2021.03.030>
- Lawrence PA, Crick FH, Munro M (1972) A gradient of positional information in an insect, *Rhodnius*. *J Cell Sci* 11:815–853. <https://doi.org/10.1242/jcs.11.3.815>
- Nakamura R, Katsuno T, Kishimoto Y, Kaba S, Yoshimatsu M, Kitamura M, Suehiro A, Hiwatashi N, Yamashita M, Tateya I, Omori K (2020) A novel method for live imaging of human airway cilia using wheat germ agglutinin. *Sci Rep* 10:14417. <https://doi.org/10.1038/s41598-020-71049-z>
- Nakamura R, Katsuno T, Tsuji T, Oyagi S, Kishimoto Y, Suehiro A, Tateya I, Omori K (2021) Airway ciliated cells regenerated on collagen sponge implants acquire planar polarities towards nearby edges of implanted areas. *J Tissue Eng Regen Med* 15:712–721. <https://doi.org/10.1002/term.3220>
- Nübler-Jung K (1987) Insect epidermis: Disturbance of supracellular tissue polarity does not prevent the expression of cell polarity. *Roux Arch Dev Biol* 196:286–289. <https://doi.org/10.1007/BF00395951>
- Randell SH, Boucher RC, University of North Carolina Virtual Lung Group (2006) Effective mucus clearance is essential for respiratory health. *Am J Respir Cell Mol Biol* 35:20–28. <https://doi.org/10.1165/rcmb.2006-0082SF>
- Sone N, Konishi S, Igura K, Tamai K, Ikeo S, Korogi Y, Kanagaki S, Namba T, Yamamoto Y, Xu Y, Takeuchi K, Adachi Y, Chen-Yoshikawa TF, Date H, Hagiwara M, Tsukita S, Hirai T, Torisawa YS, Gotoh S (2021) Multicellular modeling of ciliopathy by combining ips cells and microfluidic airway-on-a-chip technology. *Sci Transl Med* 13:1298. <https://doi.org/10.1126/scitranslmed.abb1298>
- Srivastava B, Gegg M, Lickert H, Königshoff M (2012) The Wnt/PCP pathway alters bronchial cell morphology in idiopathic pulmonary fibrosis. In: D28. Developmental signaling reborn in adult lung disease. American Thoracic Society, pp A5531–A5531. [https://doi.org/10.1164/ajrccm-conference.2012.185.1\\_MeetingAbstracts.A5531](https://doi.org/10.1164/ajrccm-conference.2012.185.1_MeetingAbstracts.A5531)
- Thomas C, Strutt D (2012) The roles of the cadherins Fat and Dachsous in planar polarity specification in *Drosophila*. *Dev Dyn* 241:27–39. <https://doi.org/10.1002/dvdy.22736>
- Tilley AE, Walters MS, Shaykhiev R, Crystal RG (2015) Cilia dysfunction in lung disease. *Annu Rev Physiol* 77:379–406. <https://doi.org/10.1146/annurev-physiol-021014-071931>
- Tsuji T, Nakamura R, Katsuno T, Kishimoto Y, Suehiro A, Yamashita M, Uozumi R, Nakamura T, Tateya I, Omori K (2018) Long-term preservation of planar cell polarity in reversed tracheal epithelium. *Respir Res* 19:22. <https://doi.org/10.1186/s12931-018-0726-y>
- Vladar EK, Bayly RD, Sangoram AM, Scott MP, Axelrod JD (2012) Microtubules enable the planar cell polarity of airway cilia. *Curr Biol* 22:2203–2212. <https://doi.org/10.1016/j.cub.2012.09.046>
- Vladar EK, Königshoff M (2020) Noncanonical Wnt planar cell polarity signaling in lung development and disease. *Biochem Soc Trans* 48:231–243. <https://doi.org/10.1042/BST20190597>
- Vladar EK, Nayak JV, Milla CE, Axelrod JD (2016) Airway epithelial homeostasis and planar cell polarity signaling depend on multiciliated cell differentiation. *JCI Insight* 1:1–18. <https://doi.org/10.1172/jci.insight.88027>
- Wallingford JB (2010) Planar cell polarity signaling, cilia and polarized ciliary beating. *Curr Opin Cell Biol* 22:597–604. <https://doi.org/10.1016/j.cub.2010.07.011>
- Warchol ME, Montcouquiol M (2010) Maintained expression of the planar cell polarity molecule Vangl2 and reformation of hair cell orientation in the regenerating inner ear. *J Assoc Res Otolaryngol* 11:395–406. <https://doi.org/10.1007/s10162-010-0209-4>
- Yang C, Axelrod J, Simon M (2002) Regulation of frizzled by fat-like cadherins during planar polarity signaling in the *Drosophila* compound eye. *Cell* 108:675–688. [https://doi.org/10.1016/s0092-8674\(02\)00658-x](https://doi.org/10.1016/s0092-8674(02)00658-x)

**Publisher's Note** Springer Nature remains neutral with regard to jurisdictional claims in published maps and institutional affiliations.

Springer Nature or its licensor (e.g. a society or other partner) holds exclusive rights to this article under a publishing agreement with the author(s) or other rightsholder(s); author self-archiving of the accepted manuscript version of this article is solely governed by the terms of such publishing agreement and applicable law.